Journal of Inventive Engineering and Technology (JIET)
ISSN: 2705-3865
Volume-5, Issue-2, pp-48-59
www.jiengtech.com
Research Paper Open Access

Backward Evaluation of the PZT Volume Fraction in PZT-Silicone Resin Composite Based on the Failure Strain and Young Modulus

N. E. Nwankwo[1], C. C. Emekwisia[2], C. N. Nwambu[3], N. H. Edeh[4], G. A. Aruya[5], and C. I. Nwoye[6]

[1,2,3,6] Chemical Systems and Data Research Laboratory, Department of Metallurgical and Materials Engineering, Nnamdi Azikiwe University, Awka, Nigeria.
[4]Department of Metallurgical and Materials Engineering, University of Lagos, Nigeria.
[5]Department of Civil Engineering, Auchi Polytechnic, Auchi, Nigeria.

Corresponding Author: *cc.emekwisia@unizik.edu.ng*

ABSTRACT : *Backward evaluation of the PZT volume fraction in PZT-silicone resin composite was achieved based on the failure strain and Young modulus of the composite, using a derived empirical model;* $\gamma = \varphi lnE_c - n\xi_c + N$. *Validity of the derived model anchored on the core model structure;* $\gamma + n\xi_c \approx \varphi lnE_c + N$, *considering that both sides of the structure are correspondingly near equal. This research presents PZT particle and silicone resin as the filler and matrix respectively. The trend and spread of results points shown in previous research significantly agrees with predicted results. Evaluated correlations between the PZT volume fraction and failure strain & Young modulus, using model-predicted results were all > 0.99. Results evaluation show that the standard error incurred in predicting the PZT volume fraction, relative to the experimental results is < 1.22%, for each value of the failure strain and Young modulus. This translates to over 98% model confidence level. Using experimental and model-predicted results, the PZT volume fraction per unit Young modulus and failure strain were 0.8316, 0.8503 & 0.8379 (%/MPa) and 1.2913, 1.3204 and 1.3012 respectively. The overall maximum deviation of the model-predicted PZT volume fraction from experimental results was 5.72%. The derived model will predict PZT volume fractions, within the experimental results range, on substituting into the model, evaluated failure strains and Young moduli, providing the boundary conditions are considered.*

KEYWORDS: *Evaluation, PZT volume fraction, PZT-silicon resin composite, failure strain, Young modulus*

Date of Submission: 12-04-2024 Date of acceptance: 17-04-2024

I. INTRODUCTION

Large-area complex curved plate structures, such as the fuselage and the wings of an aircraft, can easily experience micro-damage during service. If the micro-damage is not detected promptly, it accumulates and expands, leading to rapid structural damage, and possibly, even sudden disastrous accidents (Royon et al., 2021; Wang et al., 2021). Ultrasonic guided waves (UGW) can travel long distances evenin materials with low attenuation and are highly sensitive to slight damage along a propagation path, making them suitable for large area structural damage detection (Jiang et al., 2021). Ultrasonic guided wave technology based on piezoelectric sensors is considered a very promising technology for aircraft structural damage detection (Ricci et al., 2022). Traditional UGW sensors are made of lead zirconate titanate ($Pb(Zr0.52Ti0.48)O_3$; abbreviated PZT) ceramics, but their large density, brittleness, and small limit strain make them difficult to apply to curved structure surfaces (Zhang, 2016; Rocha et al., 2021).

In recent years, researchers have developed many new types of flexible piezoelectric materials, such as polyvinylidene fluoride (PVDF) (Kang and Cao, 2014; Jin et al., 2018), 1–3 or 2–2 piezoelectric fiber composites, and 0–3 piezoelectric composites (Pramanik and Arockiarajan, 2019; Jia et al., 2021). PVDF piezoelectric film has advantages

of small thickness and high flexibility, but its piezoelectric performance fluctuates greatly at ambient temperatures. Piezoelectric fiber composites are fine diameter piezoelectric fibers evenly arranged in a polymer, such as macro fiber composites (MFC) (Di Rito et al., 2020) and active fiber composites (AFC) (Stepinski et al., 2017). However, their fabrication is complex and their production cost is high, resulting in their limited application. The 0–3 piezoelectric composite is a material of piezoelectric particles randomly dispersed in a polymer matrix. It has broad potential applications in structural health monitoring sensors because of its low production cost, high flexibility, and effective piezoelectric properties (Yang, 2017; Arul and Rao, 2020). The low production cost and high flexibility of 0–3 piezoelectric composites make them easy to be applied to aircraft wings (Han and Kang, 2020). Many researchers have verified the feasibility of fabricating flexible piezoelectric sensors with 0–3 PZT/polymer piezoelectric composites (Sofi et al., 2022). Yang and Fritzen (2012) reviewed the research on 0–3 PZT/polymer composites over the last century, prepared a PZT/epoxy resin composite using a casting method, and explored its application in vibration mode tests. Kang and Lee (2014) prepared a PNN–PZT/epoxy resin composite and verified its application potential as a vibration sensor. Kang and Kang (2017) sprayed a suspension of PNN–PZT powder and epoxy resin composite on curved wind turbine blades using it as an acoustic emission sensor to monitor bird collision signals. Sappati and Bhadra (2020) prepared a 0–3 PZT/PDMS piezoelectric composite, studied the effects of PZT concentration on material piezoelectric properties and elastic modulus, and verified its application in pressure sensors. Han and Kang (2018) studied the effects of poling conditions and piezoelectric materials on the piezoelectric properties of a PNN–PZT/epoxy piezoelectric composite. It was used as an impact guide wave sensor to be applied in large aircraft fuselage wings. The working conditions of an aircraft structure are very complex during service, including large strain structural vibrations, hail or bird impact, and fluctuating ambient temperatures (Giurgiutiu, 2015). Sensors used for aircraft structural health monitoring must be sensitive, flexible, impact-resistant, and have service condition adaptability. For example, the failure strain cannot be less than 8,000 με (Scarponi, 2015), and the service temperature range must be at least -55–75°C (Salamone et al., 2009). Silicone resin is a semi-inorganic polymer featuring good flexibility, strong cohesion, and a low curing shrinkage rate. It also has high-temperature and high-frequency dielectric properties and temperature stability (Wang et al., 2010), making it an ideal material for a 0–3 piezoelectric composite matrix.

Previous research (Sundar et al., 2018, Burianova et. al., 2000) shows that the dielectric permittivity of the PZT ceramic reinforced epoxy is related to the volume percent PZT in composite and density of the composite. They also shows that PZT volume fraction affects the failure strain and Young modulus. However, before now, no existing mathematical expression or model has established this relationship. This therefore formed the basis for the present work to fill in the gap.

The present work aimed at developing an empirical model which will prompt a backward evaluation of the PZT volume fraction in PZT-silicone resin composite based on the failure strain and Young modulus of the composite. The gains derivable from the model include ascertaining the actual PZT content of the composite if the failure strain and Young modulus are known. With this, a PZT-silicone resin composite with varying failure strains and Young moduli can be manufactured with a pre-information of the range of PZT content required. The model if derived, shall predict the PZT volume fraction in the composite within the experimental result range, providing the input parameters are within the boundary conditions.

II. MATERIALS AND METHODS

Fabrication of a 0–3 PZT/silicone resin piezoelectric composite PZT-5A has high piezoelectric sensitivity, wide frequency response bandwidth and excellent stability to time and temperature, which means that it is more suitable for sensor materials and can be used in various environments (Eltouby et al., 2021). Therefore, PZT-5A powder was selected to prepare the piezoelectric composite.

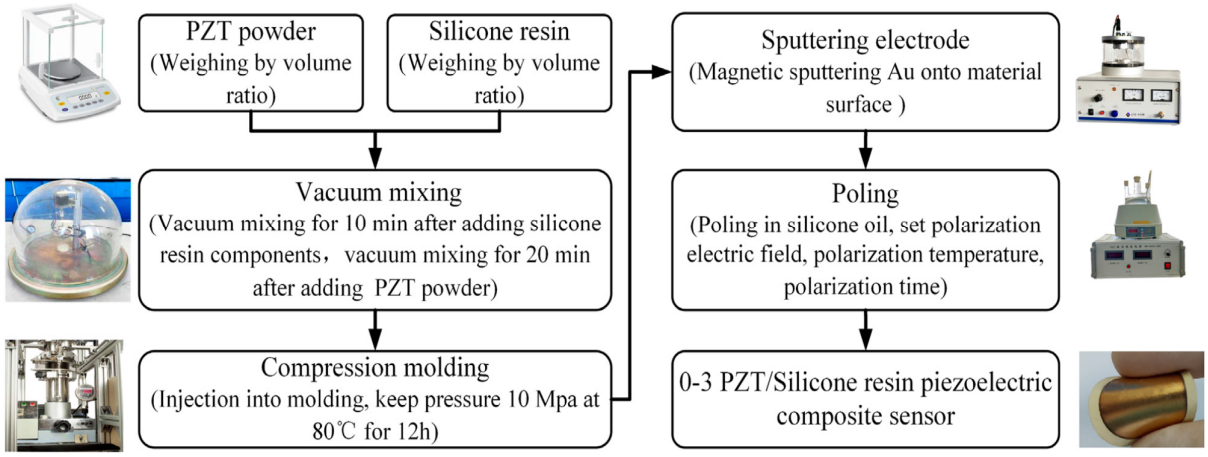

Fig. 1: Preparation process of the PZT/silicone resin piezoelectric composite

PZT-5A, provided by Yantai Xingtao Electronic Technology Co., Ltd (Yantai, China), has a density of 7.75 g/cm^3. The matrix material is 192 silicone resin produced by Ausbond (China) Co., Ltd. (Shenzhen, China), with a silicone resin density of 1.40 g/cm^3 after curing, a relative dielectric constant of 3.3, Young's modulus of 2.5 GPa, and a Shore hardness of 60 HA (Jiang et. al., 2022).

A. Preparation of a Composite

PZT powders serve as a functional phase of the PZT/ silicone resin piezoelectric composite, so its volume fraction and powder size are important parameters determining composite material properties. PZT blocks were treated by crushing, ball grinding, and screening to fabricate powders of seven different sizes: 1~15μm, 45~80μm, 90~113μm, 113~170μm, 170~212μm, 212~315μm, and 315~400μm. The preparation procedure of 0–3 PZT/silicone resin piezoelectric composites is shown in Figure 1. First, silicone resin and curing agent were mixed in a 1:1 ratio and stirred in a vacuum. Then the PZT powder was added with specified volume fractions to the composite, continuing to be stirred in a vacuum to remove bubbles and form a paste mixture. The mixture was injected into a mold and cured for 12 h at 10 MPa and 80°C. The final PZT/silicone resin piezoelectric composite was obtained after standing for 12 h. The ET500 magnetic sputter was used to fabricate the upper and the lower surface electrodes by spraying gold film. The composite material was polarized along its thickness direction in a constant temperature silicon oil bath to activate its piezoelectric properties (Jiang et. al., 2022).

B. Mechanical test on samples

Elastic modulus and failure strain the elastic modulus and failure strain were measured by tensile tests of the PZT/silicone resin composite. Generally, the lower the elastic modulus and the greater the failure strain, the better will be the flexibility of the composite material. The tests were conducted according to ISO 37:2005. The experimental equipment used is the WDW-10 universal test machine, and the specimen size is dumbbell type 3. A total of five specimens were measured in each set of experiments at a stretching rate of 2 mm/min. The elastic modulus and failure strain were calculated based on the load force and elongation of the specimen (Jiang et. al., 2022).

C. BACKWARD EVALUATION MODEL FOR PZT VOLUME FRACTION IN 0–3 PZT/SILICONE RESIN PIEZOELECTRIC COMPOSITE.

A. Model Derivation

Table 1: Variation of the input volume fraction of PZT in PZT-silicone resin composite with its Young modulus and failure strain (Jiang et. al., 2022).

(ϒ)	(ϒm)	(Ec)	(ξ_c)
35	65	6.00	19.99
38	62	6.90	18.80
40	60	7.50	18.00
43	57	10.26	17.41
45	55	12.10	17.02
48	52	16.90	12.21
50	50	20.10	9.01
53	47	24.54	7.44
55	45	27.50	6.40

Computational analysis of the experimental results shown in Table 1, resulted to Table 2 which indicate that;

$$ϒ + n\xi_c \approx \varphi \ln E_c + N \quad (1)$$

$$ϒ = \varphi \ln E_c - n\xi_c + N \quad (2)$$

The mathematical expression in (2) unveils an empirical model which gives a backward prediction of the input volume fraction of lead zirconate titanate (PZT) in PZT –silicone resin composite, based on the evaluated Young modulus and failure strain (plastic strain at failure) of the material. The variables ϒ, ξ_c and E_c are the input volume fraction of PZT (%), failure strain (%) and Young modulus (MPa) respectively. The model is referred to as Nwoye`s Model for piezo zirconate titanate input concentration in piezo zirconate titanate –silicone resin composite or Nwoye`s PIC-SIRECOM Model. The equalizing constants; n, φ and N are 0.6217, 5.9955 and 38.6875 respectively. The equalizing constant were generated using a software (Nwoye, 2008). The interaction between the constants and associated variables ensured same units on both sides of the model.

$$\xi_c = \frac{\Delta L}{L_0} \times 100\% \quad (3)$$

L_0 = Original length (mm)
ΔL = Elongation (differential between final and original length- mm)

Failure strain can be calculated using the conventional formular in (3) by substituting it, experimental input and out parameters such as original length and elongation.

Substituting (3) into (2), the PZT input volume fraction, becomes;

$$ϒ = \varphi \ln E_c - n(\Delta L 100\%. L_0^{-1}) + N \quad (4)$$

The derived model in (2) can be detailed as (4) by substituting the mathematical expressions relating the failure strain (plastic strain at failure) ξ_c during the plastic deformation into (2), providing the numerical differential between both expressions are negligible.

III. RESULTS AND DISCUSSIONS

A. Boundary and Initial Conditions

Consider PZT particles, interacting with silicone resin which is the matrix. The failure strain and young modulus of the composite are affected by PZT content of the composite. The considered range of PZT, silicone resin, failure strain and Young modulus are 35-55%, 45-65%, 6.4 -19.99% and 6.0-27.5 MPa respectively.

Table 2: Variation of $\gamma + n\xi_c$ with $\varphi \ln E_c + N$

$\gamma + n\xi_c$	$\varphi \ln E_c + N$	Differential
47.4278	49.4302	-2.0024
49.6880	50.2678	-0.5798
51.1906	50.7678	0.4228
53.8238	52.6468	1.1770
55.5813	53.6355	1.9458
55.5910	55.6386	-0.0476
55.6015	56.6782	-1.0767
57.6254	57.8749	-0.2495
58.9789	58.5578	0.4211

B. Model Validity

Results in Table 1 reveal the input and output variables of the experiment carried out to evaluate the Young moduli and failure strains in the PZT-Silicone/resin composite, at various PZT input volume fractions, using the conventional equation in (3). The table shows increased and decreased Young modulus and failure strain respectively with increase in the PZT input volume fraction. The mathematical expression in (1) is the core model structure; the basis for validity of the derived model, in that both sides of the structure are correspondingly almost equal. Table 2 is in agreement with the model structure; confirming the proximity of both sides of the structure, as shown by its evaluated components.

The derived model was also validated by comparing the predicted results with the experimental, through graphical, statistical and deviation analysis.

a. Graphical Analysis

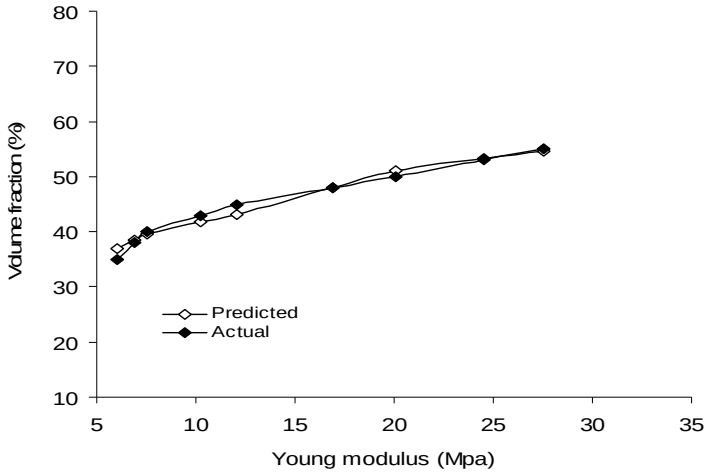

Fig.2: Comparison of PZT input volume fractions in PZT-silicone resin composite (relative to Young modulus) as evaluated from actual results and derived model

Fig. 2 and Fig. 3 show closely aligned and fitted curves of PZT input volume fraction in the composite, relative to the Young modulus and failure strain respectively. The curves represent experimental and model-predicted results. These curves are not only closely fitted, but similar in terms of the trend & spread of results point distribution. Curves from these figures show that PZT volume fraction is directly and inversely related to the Young modulus and failure strain respectively. It is expected that the highlighted relationship will emphasize positive and negative slopes respectively.

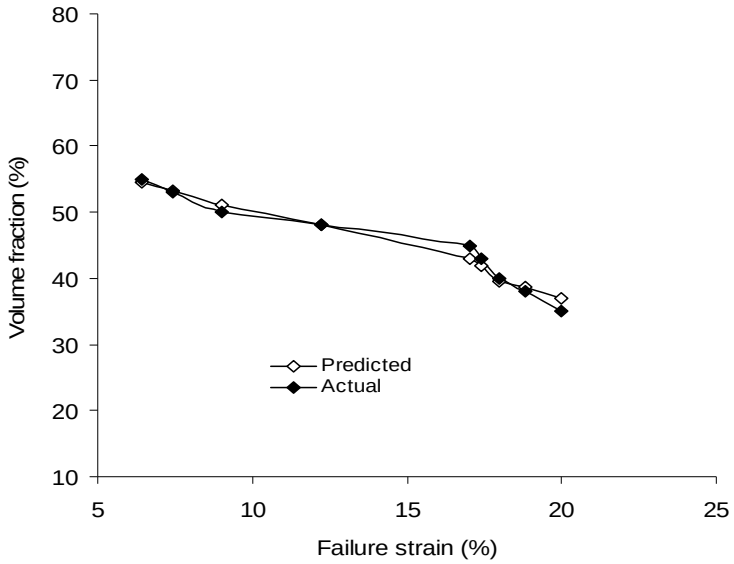

Fig.3: Comparison of PZT input volume fractions in PZT-silicone resin composite (relative to failure strain) as evaluated from actual results and derived model.

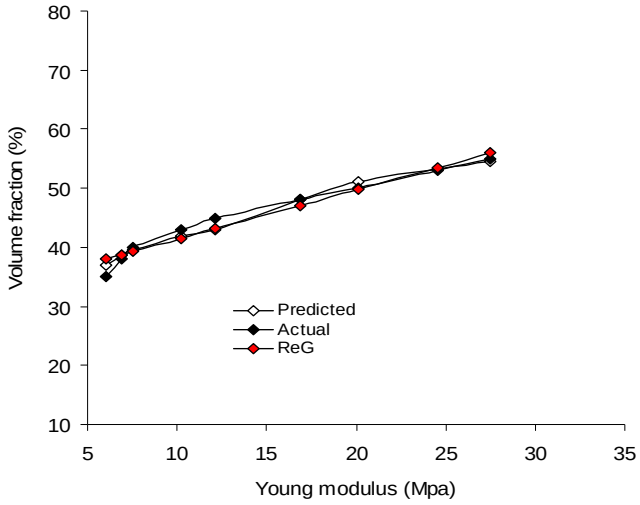

Fig. 4: Comparison of PZT input volume fractions in PZT-silicone resin composite (relative to Young modulus) as evaluated from actual results, derived model and regression model-predicted results

Fig. 4 and Fig.5 are not only similar to Fig.2 and Fig. 3 in terms of the trend of result points, but also the spread and closeness of corresponding result points. The extra features of Fig.4 and Fig.5 are the respective regression curves, which also link the PZT volume fraction to the Young modulus and failure strain respectively. The regression curves were plotted with results predicted by a standard model (regression model), based on the trend from the experimental results. The essence of plotting the regression results alongside those from the experiment and model-prediction is to verify the validity of the derived model through its level of fitness with the experimental and model-predicted already plotted. Fig.4 and Fig.5 also reveal that the associated regression curves emphasize positive and negative slopes, as a result of their direct and inverse relationships respectively.

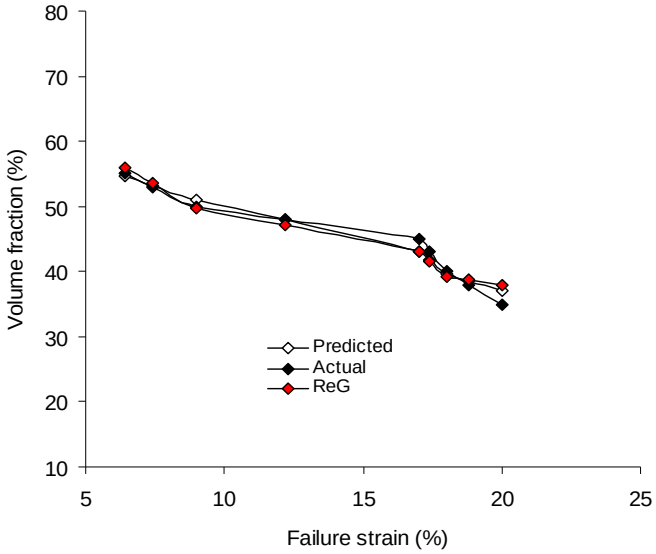

Fig.5: Comparison of PZT input volume fractions in PZT-silicone resin composite (relative to failure strain) as evaluated from actual results, derived model and regression model-predicted results.

c. Statistical Analysis

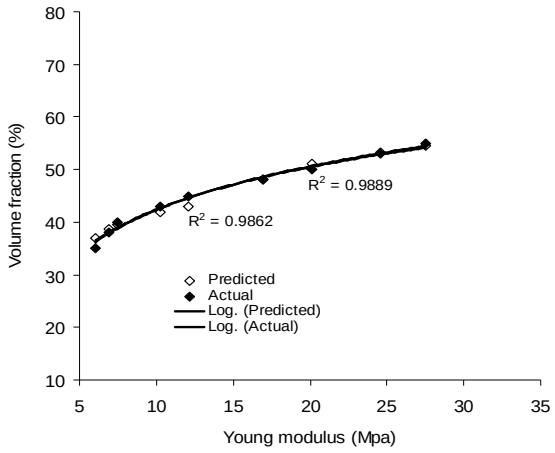

Fig.6: Coefficient of determination between PZT input volume fraction (in PZT- silicone resin composite) and Young modulus as evaluated from actual results and derived model.

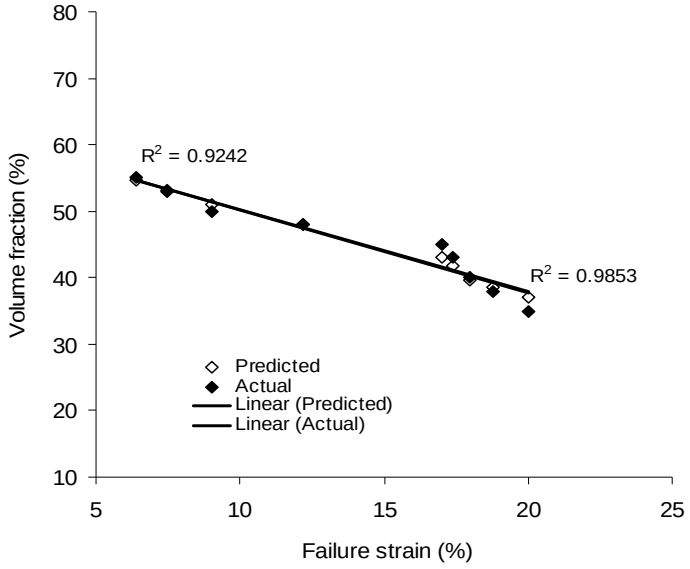

Fig.7: Coefficient of determination between PZT input volume fraction (in PZT - silicone resin composite) and failure strain as evaluated from actual results and derived model.

The correlations between PZT input volume fraction and Young modulus & failure strain were evaluated from the coefficients of determination R^2 shown in Fig.6 & Fig. 7 as 0.9944 and 0.9931 & 0.9926 and 0.9614, using model-predicted and experimental results respectively. Comparative analyses of these results indicate that data points distribution from model prediction show greater alignment and better fitted lines than those from the experiment. However, on pairing both results, they show very close alignment.

Statistical analysis involving prediction of PZT input volume fraction, relative to the experimental results indicates that the incurred overall standard error is < 1.22%, for every change in the Young modulus and failure strain in the composite. This gives a model confidence level above 98%.

d. Deviation Analysis

Table 3: Differential between experimentally determined and model-predicted PZT input concentration γ_ε and γ_M respectively.

γ_ε	$\Delta\gamma = \gamma_M - \gamma_\varepsilon$
35	-2.0024
38	-0.5798
40	0.4228
43	1.1770
45	1.9458
48	-0.0476
50	-1.0767
53	-0.2495
55	0.4211

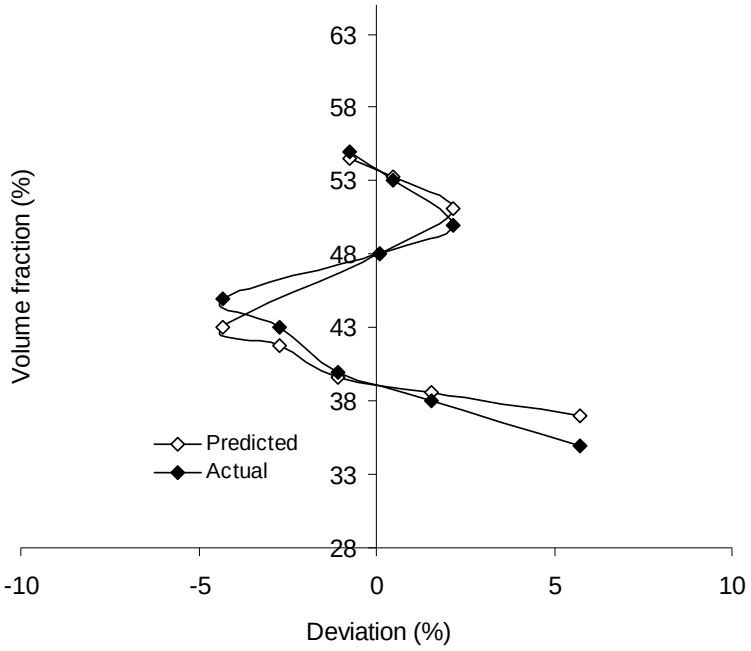

Fig. 8: Variation of model-predicted of PZT input volume fraction with its corresponding deviation from experimental results.

Table 3 shows the differential between experimentally determined PZT input volume fraction and model prediction. Some evaluated differentials are quite negligible, indicating that the derived model predicted values are almost the same as corresponding experiment results. The positive and negative differentials show increased and decreased model-predicted values respectively, relative to the corresponding experimental result. The differentials involving the core model structure; Table 2 and experimental and model-predicted model; Table 3 is equal. This affirms the validity of the derived model.

The deviation Dv, of model-predicted PZT volume fraction from the corresponding experimental result was evaluated from the expression.

$$D_v = \left(\frac{\gamma_m - \gamma_\varepsilon}{\gamma_\varepsilon}\right) \times 100 \qquad (5)$$

Where

γ_ε and γ_m are PZT volume fraction of the composite evaluated from experiment and model-predicted results respectively.

Fig. 8 shows the least and highest deviations of the model-predicted PZT input volume fraction as 0.1 and 5.72% respectively. These deviations correspond to the PZT input volume fraction: 48.0476 & 37.0024%, failure strain: 12.21 & 19.99% and Young modulus: 16.9 & 6.0 MPa respectively. Furthermore, the figure shows the overall maximum deviation of model-predicted PZT input volume fraction (from experimental values) as 5.72%. This gives over 94% operational model confidence levels. At each corresponding results set, other discrepancies (in percent) between the experimental and model-predicted results are also shown in the figure. It is strongly believed, based on evaluated correlations, standard error and maximum deviation that the overall model confidence level places between 94 and 99%.

Correction factor which overcomes the deviation is calculated as the negative of equation (5)

$$C_f = -\left(\frac{\gamma_m - \gamma_\varepsilon}{\gamma_\varepsilon}\right) \times 100 \qquad (6)$$

PZT input volume fraction per unit Young modulus of PZT-Silicone resin composite γ_{Ec} (%/Mpa) was calculated from the expression;

$$\gamma_{Ec} = \frac{\gamma}{E_c} \qquad (7)$$

Re-written as

$$\gamma_{Ec} = \frac{\Delta\gamma}{\Delta E_c} \qquad (8)$$

The expression (8), is detailed as

$$\gamma_{Ec} = \frac{\gamma_2 - \gamma_1}{E_{c2} - E_{c1}} \qquad (9)$$

Where

$\Delta\gamma$ = Change in the PZT input volume fraction γ_2, γ_1 at two Young moduli values of the composite E_{c2}, E_{c1}.

A plot of points (6.9, 38) & (24.54, 53), (6.9, 38.5798) & (24.54, 53.2495) and (6.9, 38.7329) & (24.54, 53.514) as shown in Figure 4, designated as (E_{c1}, γ_1) and (E_{c2}, γ_2) for experimental, derived model and regression model-predicted results, and substituting them into the expression (9), gives the slopes: 0.8316, 0.8503 and 0.8379 (%/Mpa), as their respective PZT input volume fraction per unit Young modulus of the composite.

PZT input volume fraction per unit failure in PZT-Silicone resin composite $\gamma_{\xi c}$ was calculated from the expression;

$$\gamma_{\xi c} = \frac{\gamma}{\xi_c} \qquad (10)$$

Re-written as

$$\gamma_{\xi c} = \frac{\Delta\gamma}{\Delta\xi_c} \qquad (11)$$

The expression (11), is detailed as

$$\gamma_{\xi c} = \frac{\gamma_2 - \gamma_1}{\xi_{c2} - \xi_{c1}} \qquad (12)$$

Where;

$\Delta\xi_c$ = Change resulting from two failure strain values from the composite ξ_{c2}, ξ_{c1}

Plotting points (18.8, 38) & (7.44, 53), (18.8, 38.5798) & (7.44, 53.2495) and (18.8, 38.7329) & (7.44, 53.514) as shown in Fig. 5, designated as (ξ_{c1}, γ_1) and (ξ_{c2}, γ_2) for experimental, derived model and regression model-predicted results, and substituting them into the expression (12), gives the slopes: -1.2913, -1.3204 and -1.3012, as their respective PZT input volume fraction per unit failure strain in the composite. The real PZT input volume fraction per unit failure strain in the composite are the magnitudes of the results; 1.2913,1.3204 and 1.3012. The negative signs preceding the values are just indications that the slopes involved are negative.

IV CONCLUSION

Backward evaluation of the PZT volume fraction in PZT-silicone resin composite was achieved based on the failure strain and Young modulus of the composite, using a derived empirical model; $\gamma = \varphi \ln E_c - n\xi_c + N$.
Validity of the derived model anchored on the core model structure; $\gamma + n\xi_c \approx \varphi \ln E_c + N$, considering that both sides of the structure are correspondingly near equal. Evaluated correlations between the PZT volume fraction and failure strain & Young modulus, using model-predicted results were all > 0.99. Results evaluation show that the standard error incurred in predicting the PZT volume fraction, relative to the experimental results is < 1.22%, for each value of the failure strain and Young modulus. This translates to over 98% model confidence level. Using experimental and model-predicted results, the PZT volume fraction per unit Young modulus and failure strain were 0.8316, 0.8503 & 0.8379 (%/Mpa) and 1.2913, 1.3204 and 1.3012 respectively. The overall maximum deviation of the model-predicted PZT volume fraction from experimental results was 5.72%. The derived model will predict PZT volume fractions, within the experimental results range, on substituting into the model, evaluated failure strains and Young moduli, providing the boundary conditions are considered.

REFERENCES

Arul, K. T., and Rao, M. S. R. (2020). Ferroelectric properties of flexible PZT composite films. J. Phys. Chem. Solids 146, 109371. doi:10.1016/j.jpcs.2020.109371.

Burianova, L., Hana, P., Panos, S., Kulek, J., & Tyagur, Y. I. (2000). Piezoelectric, Dielectric and Pyroelectric Properties of 0-3 Ceramic-Polymer Composites. Ferroelectrics, 241(1–4), 59–66.

Di rito, G., Chiarelli, M. R., and Luciano, B. (2020). Dynamic modelling and experimental characterization of a self-powered structural health-monitoring system with MFC piezoelectric patches. Sensors 20, 950. doi:10.3390/s20040950.

Eltouby, P., Shyha, I., Li, C., and Jibran, K. H. A. L. I. Q. (2021). Factors affecting the piezoelectric performance of ceramic-polymer composites: A comprehensive review. Ceram. Int. 47, 17813–17825. doi:10.1016/j.ceramint.2021.03.126.

Giurgiutiu, V. (2015). Published. SHM of aerospace composites—challenges and opportunities. Proc. Compos. Adv. Mater. Expo 2015, 1–15. Dallas, TX: CAMX.

Han, D.-H., and Kang, L.-H. (2018). Piezoelectric characteristics of PNN-PZT/Epoxy paint sensor according to the poling conditions. Sensors Actuators A Phys. 269, 419–426. doi:10.1016/j.sna.2017.12.005.

Han, D.-H., and Kang, L.-H. (2020). Piezoelectric properties of paint sensor according to piezoelectric materials. Funct. Compos. Struct. 2, 025002. doi:10.1088/2631-6331/ab90e1.

Jiang, S., Shen, Y., Wang, S., Peng, Y., and Liu, Y. (2021). The effect of piezoelectric fiber rosette configurations on lamb wave direction detection for damage localization. J. Sensors 2021, 1–10. doi:10.1155/2021/9918049.

Jiang, S., Shen, Y., Wang, S., Zhi, Y., and Han, B. (2022). Properties of novel 0–3 PZT/silicone resin flexible piezoelectric composites for ultrasonic guided wave sensor applications. Front. Mater. 9:958775. doi: 10.3389/fmats.2022.958775, 1-14.

Jin, L., Ma, S., Deng, W., Yan, C., Yanga, T., Chu, X., Tiang, G., Xiong, D., Lu, J., and Yang, W., (2018). Polarization free high-crystallization β-PVDF piezoelectric nanogenerator toward self-powered 3D acceleration sensor. Nano Energy 50, 632–638. doi:10.1016/j.nanoen.2018.05.068.

Jia, H., Li, H., Lin, B., Hu, Y., Peng, L., Xu, D., Cheng X. (2021). Fine scale 2-2 connectivity PZT/epoxy piezoelectric fiber composite for high frequency ultrasonic application. Sensors Actuators A Phys. 324, 112672. doi:10.1016/j.sna.2021.112672.

Kang, G.-D., and Cao, Y.-M. (2014). Application and modification of poly (vinylidene fluoride)(PVDF) membranes–a review. J. Membr. Sci. 463, 145–165. doi:10.1016/j.memsci.2014.03.055.

Kang, L.-H., and Lee, J.-R. (2014). Piezoelectric paint sensor for impact and vibration monitoring. 7th European workshop on structural health monitoring. Lacité, nantes, France: More info at open access database. Chonbuk: Korea.

Kang, S.-H., and Kang, L.-H. (2017). Development of wireless bird collision monitoring system using 0-3 piezoelectric composite sensor on wind turbine blades. J. Intelligent Material Syst. Struct. 29, 3426–3435. 1045389X17730925. doi:10.1177/1045389x17730925.

Nwoye, C. I. (2008). Data Analytical Memory; C-NIKBRAN.

Pramanik, R., and Arockiarajan, A. (2019). Effective properties and nonlinearities in 1-3 piezocomposites: A comprehensive review. Smart Mat. Struct. 28, 103001. doi:10.1088/1361-665X/ab350a.

Ricci, F.,Monaco, E., Boffa, N., Maio, L., and Memmolo, V. (2022). Guided waves for structural health monitoring in composites: A review and implementation strategies. Prog. Aerosp. Sci. 129, 100790. doi:10.1016/j.paerosci.2021.100790.

Rocha, H., Semprimoschnig, C., and Nunes, J. P. (2021). Sensors for process and structural health monitoring of aerospace composites: A review. Eng. Struct. 237, 112231. doi:10.1016/j.engstruct.2021.112231.

Royon, M., Jamon, D., Blanchet, T., Royer, F., Vocanson, F., Marin, E., Morana, A., Boukenter, A., Ouerdane, Y., Jourlin, Y., Evenblij, R., Van Leest, T., De Smet, M., and Girard, S.(2021). Sol–gel waveguide-based sensor for structural health monitoring on large surfaces in aerospace domain. Aerosp. (Basel). 8, 109. doi:10.3390/aerospace8040109.

Salamone, S., Bartoli, I., Scalea, F. L. D., and Coccia, S. (2009). Guided-wave health monitoring of aircraft composite panels under changing temperature. J. Intell. Mat. Syst. Struct. 20, 1079–1090. doi:10.1177/1045389X08101634.

Scarponi, C. (2015). Hemp fiber composites for the design of a Naca cowling for ultra-light aviation. Compos. Part B Eng. 81, 53–63. doi:10.1016/j.compositesb.2015.06.001.

Sappati, K. K., and Bhadra, S. (2020). Flexible piezoelectric 0–3 PZT-PDMS thin film for tactile sensing. IEEE Sens. J. 20, 4610–4617. doi:10.1109/JSEN.2020.2965083.

Sofi, A., Jane Regita, J., Rane, B., and Lau, H. H. (2022). Structural health monitoring using wireless smart sensor network – an overview. Mech. Syst. Signal Process. 163, 108113. doi:10.1016/j.ymssp.2021.108113.

Stepinski, T., Mańka, M., and Martowicz, A. (2017). Interdigital lamb wave transducers for applications in structural health monitoring. NDT E Int. 86, 199–210. doi:10.1016/j.ndteint.2016.10.007.

Sundar, U., Banerjee, S., & Cook-C, K. (2018). Piezoelectric and Dielectric Properties of PZT-Epoxy Composite Thick Films. Academic Journal of Polymer Science, 1(5), 555574. DOI: 10.19080/AJOP.2018.01.555574

Wang, X., Lu, H., Wang, H., and Feng, S. (2010). Synthesis and photophysical properties of rare earth-containing luminescent silicone resin from cooperative molecular design and assembly. J. Non-Crystalline Solids 356, 1581–1586. doi:10.1016/j.jnoncrysol.2010.05.059.

Wang, Y., Hu, S., Xiong, T., Huang, Y., and Qiu, L. (2021). Recent progress in aircraft smart skin for structural health monitoring. Struct. Health Monit. 14759217211056831, 147592172110568. doi:10.1177/14759217211056831.

Yang, C. (2017). Distributed piezoelectric transducers and their applications in structural health monitoring. Dissertation/Doctor's degree. Siegen: University of Siegen.

Yang, C., and Fritzen, C. P. (2012). Piezoelectric paint: Characterization for further applications. Smart Mat. Struct. 21, 045017. doi:10.1088/0964-1726/21/4/045017.

Zhang, Y. (2016). In situ fatigue crack detection using piezoelectric paint sensor. J. Intelligent Material Syst.